

# Novel multifocus tomography for measurement of microstructured and multicore optical fibers

Andrew D. Yablon\*

Interfiber Analysis, 8 Manns Hill Crescent, Sharon, MA, USA 02067

## ABSTRACT

A novel multifocus tomographic algorithm for reconstructing an optical fiber's cross sectional refractive index distribution from transverse projections is described. This new algorithm is validated against measurements of both microstructured and multicore optical fibers, which were not previously measurable. Optical fiber tomographic measurements recently made by several research groups using different technologies have all suffered from the same limitation, namely that typical fiber diameters (several hundred microns) exceed the imaging depth-of-field (approximately one micron) by several orders of magnitude. The new algorithm combines data acquired from a multiplicity of focal planes to overcome this limitation, yielding measurements with extremely fine spatial resolution over large transverse dimensions, thereby providing the first-ever high quality measurements of microstructured and multicore fibers. This new measurement approach is broadly applicable to any tomographic problem in which the depth-of-field is greatly exceeded by the transverse dimension of the specimen. Many types of transverse optical fiber measurement technologies, including interference microscopy, quantitative phase microscopy (QPM), residual stress measurement, differential interference contrast (DIC) microscopy, and spontaneous emission tomography will benefit from this new algorithm, which will greatly facilitate characterization of optical fibers for high-power applications.

**Keywords:** optical fiber characterization, tomography, multi-core optical fibers, microstructured optical fibers

## 1. INTRODUCTION

### 1.1 Motivation

Over the past several years, various research groups<sup>1-9</sup> have reconstructed the complete two-dimensional cross section of an optical fiber sample from one-dimensional transverse projections acquired at a multiplicity of fiber angular orientations. The inverse Radon transform<sup>10</sup>, or a mathematically analogous algorithm, is used to synthesize the one-dimensional projections into a single two-dimensional cross section. Typically the refractive index is measured<sup>1-4,7-9</sup>, although residual stress<sup>5,7-9</sup> or the transverse distribution of rare-earth dopant<sup>11</sup> may also be measured. While two-dimensional measurements can be made at a cleaved fiber end-face, two-dimensional tomographic reconstructions from one-dimensional transverse projection data is preferable because such transverse measurements are inherently non-destructive, and therefore they can be used to map out variations along the length of a fiber, for example near a fusion splice<sup>8,9</sup>, a physical taper, or even a fiber grating. Furthermore, cleaving artificially relieves internal stresses, thereby distorting the measurement, and cleave defects compromise measurement accuracy.

However, fine spatial resolution requires a high numerical aperture (NA) imaging objective lens and therefore only a narrow slice from within the fiber's cross-section can be in focus in any one-dimensional projection. Due to this limitation, high resolution two-dimensional tomographic transverse fiber measurements could only be obtained for fibers in which any azimuthal asymmetries were relatively close to the fiber's center (where a consistent focus could be maintained), so multicore and microstructured optical fibers in particular could not previously be measured effectively using transverse techniques.

In this paper I describe a new algorithm, distinct from the inverse Radon transform and its mathematical equivalents, that overcomes this limitation by synthesizing one-dimensional data acquired at a multiplicity of focal positions and a multiplicity of angular orientations to yield high-resolution two-dimensional data on a variety of non-azimuthally symmetric fiber samples including multi-core and microstructured optical fibers. Although only transverse interferometry<sup>6</sup> results are shown here, the new algorithm is broadly applicable to a wide variety of transverse optical fiber measurement technologies<sup>1-5,7-9</sup>.

\*andrew\_yablon@interfiberanalysis.com; phone 1 781 806-0659; fax 1 973 488-7134; www.interfiberanalysis.com

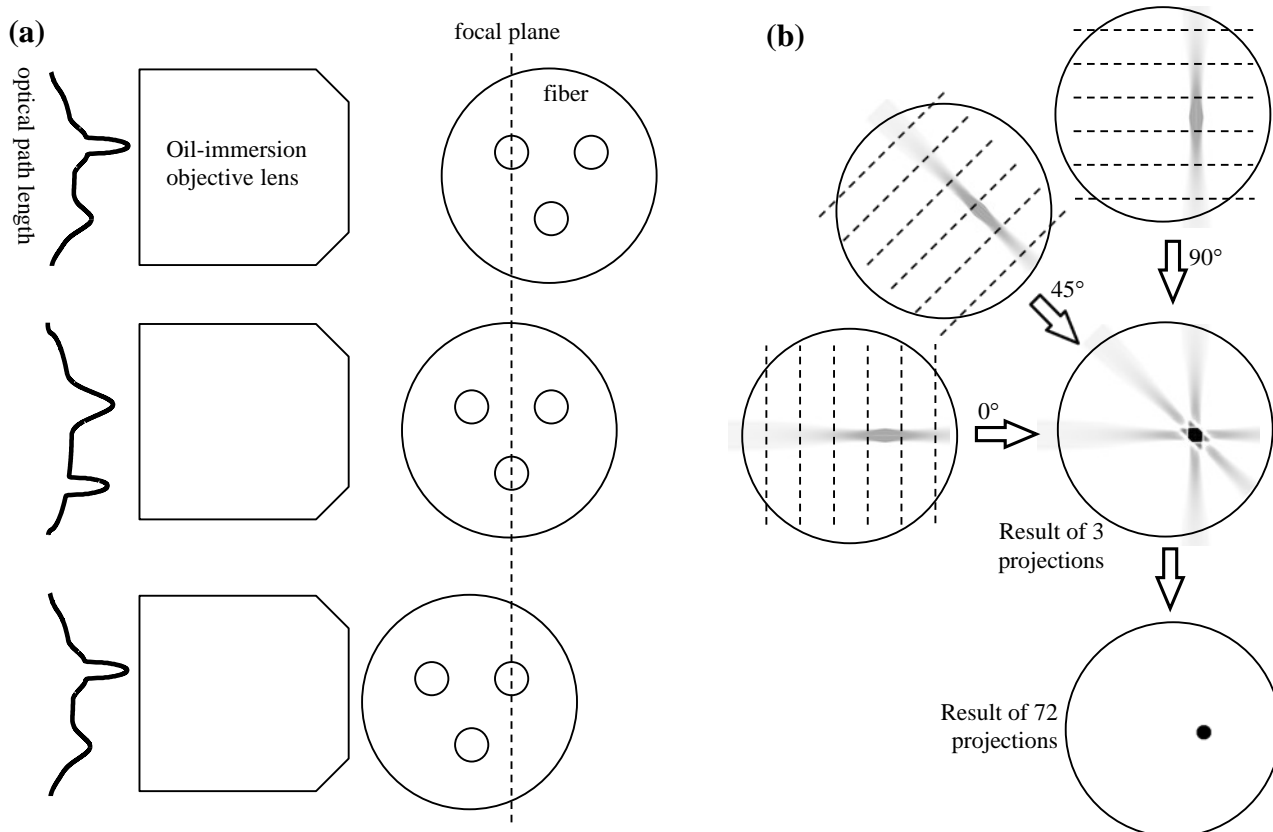


Figure 1. (a) Schematic illustration of the one-dimensional optical path length data obtained from a hypothetical three-core optical fiber (three-core fiber and objective lens both shown in cross section) at one particular rotation angle and (b) graphical illustration of the novel algorithm described here applied to several distinct projection angles ( $0^\circ$ ,  $45^\circ$ , and  $90^\circ$ )<sup>12</sup>. At far left the one-dimensional optical path length projections are seen to depend upon the displacement between the focal plane of the oil-immersion objective lens and the fiber. At right the dashed lines in (b) schematically illustrate the distinct focal plane locations comprising each matrix of filtered projections. A crucial feature of the new algorithm is that the projections acquired at each individual angle vary as a function of focal position (contrast with Figure 25-17 in reference<sup>13</sup>)

## 1.2 Algorithm

Figure 1(a) schematically illustrates the effect of finite depth-of-field on transverse one-dimensional projections of a non-azimuthally symmetric optical fiber, in this case a hypothetical three-core fiber. In this illustrative case a one-dimensional optical path length across the fiber sample is measured with an interferometer<sup>6</sup> (not shown). The depth-of-field for typical objective lenses used to transversely image optical fibers is on the order of a micron or less, whereas the typical transverse dimension of the fiber itself is on the order of hundreds of microns. Therefore it is impossible for the objective lens to be simultaneously focused on all portions of the fiber and the fine details of the measured projection will depend upon the relative displacement between the objective lens and the fiber it is imaging. In Figure 1(a) the precise details of the one-dimensional optical path length projection depend upon which core is aligned within the objective's focal plane. Previous investigations only considered the projection corresponding to the objective lens focused on the center of the fiber (middle of Figure 1(a)), although this implies that features far from the fiber center will be defocused and therefore poorly rendered in the final two-dimensional result. It is also important to note that out-of-focus features are superposed with in-focus features, thereby making them impossible to separate from each other.

Instead of *selecting* a single focal position, the new algorithm utilizes *all* of them: a large number of one-dimensional optical path length projections are acquired at video rate while scanning the fiber through the objective lens focal plane. The conventional inverse Radon transform operates on only a single projection whereas the new algorithm assembles each distinct projection acquired at a distinct focal position into a matrix of projections. As with the inverse Radon

transform, a conventional “Ram-Lak” filter<sup>10,14</sup> is applied to each individual projection in the matrix to ensure that the conversion from measured transverse projections to a reconstructed radial coordinate system is accomplished correctly. The resulting filtered matrices obtained from each angular orientation are accumulated in a unified coordinate system as shown in Figure 1(b) to reveal the accurate two-dimensional cross section of the fiber. It is critical that each filtered matrices be correctly positioned with respect to each other. To this end, special software detected the cladding edges of the fiber in the one-dimensional projections to determine a transverse center point and also detected the focal position at which the cladding edge was most sharply focused, thereby determining the center point of the focal scans.

### 1.3 Implementation

For the results described here the fiber sample was fixtured across one arm of a previously described Mach-Zehnder interferometer<sup>6</sup> with the aid of a computer controlled x-y-z translation stage that could also rotate the fiber about its longitudinal axis ( $\theta$ ). This interferometer could measure optical path lengths at a variety of different measurement wavelengths<sup>15</sup> (results are presented here at several wavelengths ranging from 632.8 nm to 2000 nm). The oil-immersion objective lens used to image the fiber had an NA of about 1.0 and a depth-of-field of only about 1 micron. The fiber was optically coupled to the high-NA oil-immersion objective lens by refractive index oil. Any polymer coating must be removed from the fiber inside the measurement zone and any air holes inside the fiber must be infused with refractive index oil, in both cases to avoid phase discontinuities associated with the strong refractive index contrast across the boundary.

The fiber was discretely rotated through a full 360° rotation in angular step increments of 5° (72 distinct angular positions). At each angular position optical path length projections were acquired at video rate as the fiber was continuously scanned through the focal plane of the objective lens. 200 distinct projections were acquired over a total scan distance of about 260 microns, corresponding to a focal step size of about 1.3 microns. Therefore a complete acquisition yielded 72×200=14,400 individual distinct one-dimensional optical path length projections. Data acquisition required approximately 30 minutes and data processing required about 2 hours.

Results are presented for a diverse variety of microstructured and multi-core optical fiber types, including both form- and stress-birefringent polarization-maintaining (PM) microstructured optical fibers as well as fibers including air holes and/or solid inclusions. A comparison between the known refractive index of the oil surrounding the fiber and the oil infused in the airholes shows that the new algorithm correctly measures the known refractive index difference.

## 2. RESULTS

Figure 2(a) shows the measured  $\Delta n$  at 850 nm measurement wavelength in false color for a four-core optical fiber (*FM4C1500*) kindly provided by *Fibercore Ltd.* In this paper,  $\Delta n$  refers to the difference between the local refractive index and refractive index oil surrounding the fiber. Even though the fiber’s cores were about 35 microns away from the fiber’s center, they were well resolved by the new algorithm. Figure 2(b) shows one-dimensional refractive index profiles for each of the four cores. The center-dip or “burn-off” region (a vestige of the manufacturing process) is evident inside the center of each core. The spatial resolution of the result is evidently on the order of about one micron.

Figure 3(a) shows the  $\Delta n$  in false color measured at 632.8 nm for an endlessly single-mode air-silica microstructured optical fiber (*NKT Photonics ESM-12B* purchased from *Thorlabs, Inc.*). The fiber was surrounded by a high refractive index oil ( $n=1.461$ ) and its airholes were infused with low refractive index oil ( $\Delta n=1.454$ ). The  $\Delta n$  between the surrounding oil and the oil in the holes was measured to be 0.007 as expected, thereby demonstrating the accuracy of the new algorithm. No symmetry was assumed for this (or any other) measurement. While weak measurement artifacts are evident as geometric patterns in the pure silica cladding between the holes, the remarkable fidelity of the results presented here should be compared to recent measurements of very similar endlessly-single-mode air-silica microstructured fibers in references<sup>3,7</sup>. Micron scale resolution was evidently achieved at distances as far as 47 microns from the fiber center.

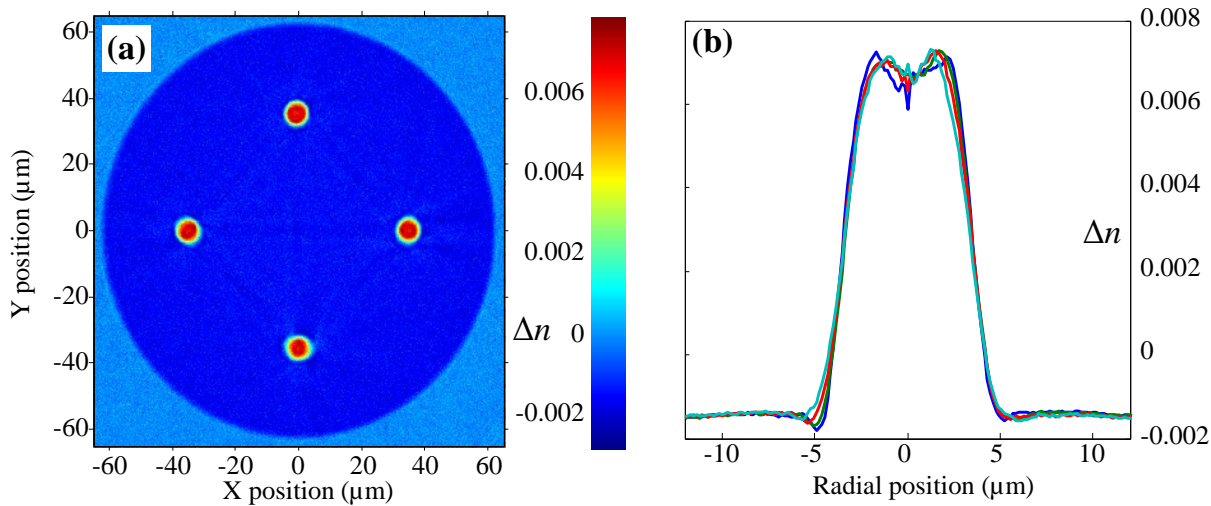


Figure 2. (a) Measurement<sup>16</sup> of a four core multicore fiber (*FM4C15000*) at 850 nm using the new tomographic algorithm with a false color representation for the local  $\Delta n$  and (b) individual one-dimensional core refractive index profiles extracted from the two-dimensional data. The region outside the fiber is reference refractive index oil. Each core is about 35 microns away from the fiber center and 50 microns away from its closest neighbor. Note the presence of a central dip or “burn-off” region in the center of all four cores. Fiber sample kindly provided by *Fibercore, Ltd.*

Figure 3(b) shows a false color close-up view of the  $\Delta n$  measured at 632.8 nm for a endlessly single-mode PM optical fiber (*NKT Photonics PM-1550* purchased from *Thorlabs, Inc.*). The fine details of the microstructure, including the two large airholes responsible for the form birefringence of this fiber, are well resolved.

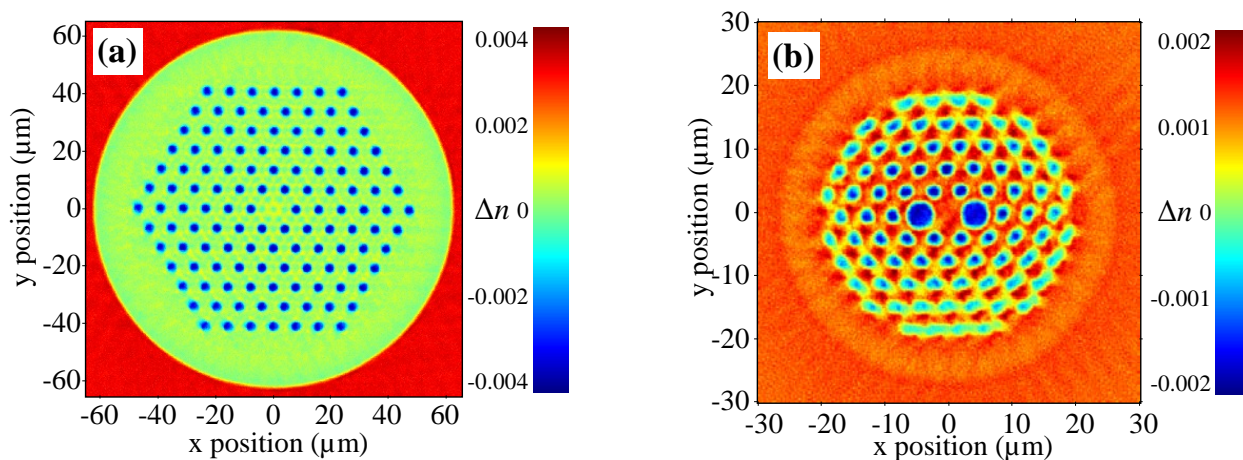


Figure 3. (a) Measurement of an “endlessly single-mode” air-silica microstructured optical fiber (*NKT Photonics ESM-12B* purchased from *Thorlabs, Inc.*) using the new tomographic algorithm<sup>12</sup> and (b) measurement of an “endlessly single-mode” form-birefringent PM air-silica microstructured optical fiber (*NKT Photonics PM-1550* purchased from *Thorlabs, Inc.*) using the new tomographic algorithm<sup>16</sup> (both measurements performed at 632.8 nm). Refractive index oil was infused into the holes of both fibers. Note that the false color scale and the spatial magnification is different for each fiber. The measured  $\Delta n$  agrees with the nominal refractive index of the oil inside the air holes and surrounding the optical fibers.

Figure 4(a) shows a photograph of a microstructured optical fiber preform containing an irregular collection of glass rods (no air holes) manufactured by XLIM Laboratory in Limoges, France. The  $\Delta n$  of the fiber drawn from this preform is depicted in false color in Figure 4(b). Fine features located dozens of microns from the fiber center are well resolved by the new algorithm. The hexagonal yellowish region in the center of the fiber is seen to have a slightly lower refractive index than the surrounding reddish inner cladding region.

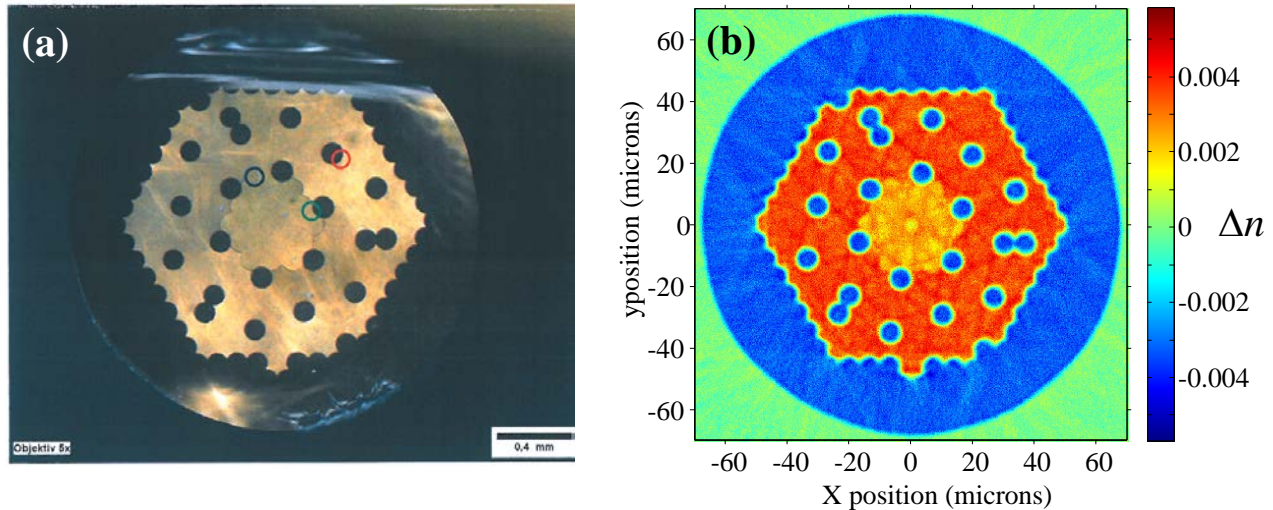


Figure 4. Comparison between (a) photograph of preform for a microstructured fiber and (b) corresponding fiber refractive index measurement result obtained at 1000 nm using the new tomographic algorithm with local  $\Delta n$  rendered in false color. The transverse dimension of the preform at left is evidently about 16 times larger than the drawn fiber sample at right. This sample contains no airholes but instead both low- and high-refractive index glass regions. Fiber sample and photograph kindly provided by *XLIM Laboratory*, Limoges, France.

Figure 5(a) shows a false color close-up view of the  $\Delta n$  measured at 2000 nm for leakage channel fiber (LCF) kindly provided by Prof. L. Dong's research group at Clemson University. This fiber includes large diameter extremely low refractive index rods (*blue*) that require measurement at long wavelength to avoid phase ambiguities when interpreting the interferometer's fringes. The radial lines in this false color image are measurement artifacts associated with phase ambiguities at the edges of the low-refractive index rods.

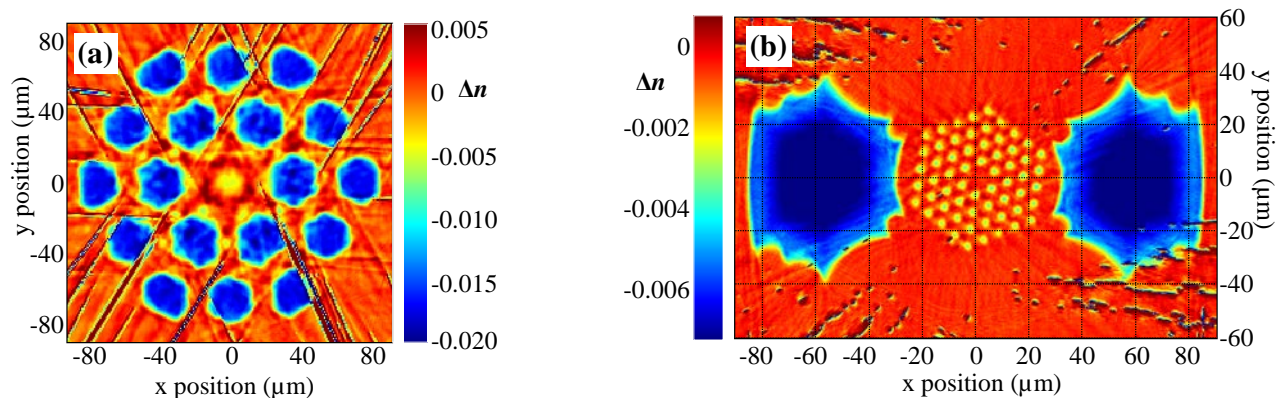


Figure 5. At left (a) two-dimensional measurement of a leakage channel fiber (LCF) measured at 2000 nm and (b) at right a PM air-silica microstructured optical fiber (*NKT Photonics LMA-PM-10* purchased from *Thorlabs, Inc.*) measured at 632.8 nm<sup>16</sup>. Note that image magnification and false color scale differ between the plots. LCF kindly provided by Prof. L. Dong's research group at Clemson University.

Figure 5(b) shows a false color close-up view of the  $\Delta n$  measured at 632.8 nm for a PM microstructured fiber (*NKT Photonics LMA-PM-10* purchased from *Thorlabs, Inc.*). The hexagonal array of yellow holes in the center of the fiber are oil-filled air holes. Unlike the fiber in Figure 3(b), this fiber relies upon solid stress rods (*blue*) to produce birefringence, although the measurement revealed that these stress rods are irregularly shaped. Furthermore, the stress rods are not rotationally aligned to the symmetry angles of the fine air hole microstructure at the center of the fiber. The dark lines visible at larger radius are measurement artifacts associated with phase ambiguities.

### 3. DISCUSSION

The results from the previous section show that the new tomographic algorithm described here is capable of providing micron-scale spatial resolution over transverse dimensions of 100 microns. This was achieved despite the fact that the imaging objective lens had a depth-of-field approximately two orders of magnitude smaller than the transverse dimension of the object. While small artifacts can sometimes be observed in the measured data, the details of the fiber's microstructure, including subtle imperfections, can be readily measured. Most importantly, the algorithm was validated against known refractive index differences.

While all of the results shown here concern measurement of refractive index with the aid of transverse interferometry, the algorithm is quite general and suitable for any tomographic measurement technique in which the imaging depth-of-field is substantially smaller than the transverse dimension of the object<sup>12</sup>. For this reason the new tomographic algorithm described here is applicable to measurement of refractive index using techniques other than transverse interferometry such as Quantitative Phase Microscopy (QPM)<sup>1,7-9</sup>, Diffraction Tomography<sup>3</sup>, or Differential Interference Contrast (DIC) microscopy<sup>4</sup> as well as measurement of fiber residual elastic stress<sup>5,7-9</sup>, or measurements of the transverse distribution of rare-earth dopant<sup>11</sup>. Three-dimensional measurements of optical fiber samples<sup>4,8,9</sup> are obtainable by repeating the fundamental two-dimensional measurement along a length of optical fiber. Since the algorithm here is generally applicable to any cylindrical object, it could conceivably be used to map out the spatial variations in an optical fiber preform, or even of materials flowing inside a capillary tube.

### REFERENCES

- [1] Barty, A., Nugent, K. A., Roberts, A. and Paganin, D., "Quantitative phase tomography," *Optics Communications* 175(4-6), 329-336 (2000).
- [2] Bachim, B. L., Gaylord, T. K., "Microinterferometric optical phase tomography for measuring small, asymmetric refractive-index differences in the profiles of optical fibers and fiber devices," *Applied Optics* 44(3), 316-327 (2005).
- [3] Gorski, W. and Osten, W., "Tomographic imaging of photonic crystal fibers", *Optics Letters* 32(14), 1977-1979 (2007).
- [4] Dragomir, N. M., Goh, X. M., and Roberts, A., "Three-Dimensional Refractive Index Reconstruction With Quantitative Phase Tomography," *Microscopy Research and Technique* 71(1), 5-10 (2008).
- [5] Kniazewski, P. Kozacki, T., and Kujawinska, M., "Inspection of axial stress and refractive index distribution in polarization-maintaining fiber with tomographic methods," *Optics and Lasers in Engineering* 47(2), 259-263 (2009).
- [6] Yablon, A. D., "Multi-Wavelength Optical Fiber Refractive Index Profiling by Spatially Resolved Fourier Transform Spectroscopy," *IEEE Journal of Lightwave Technology* 28(4), 360-365 (2010).
- [7] Jenkins, M. H. and Gaylord, T. K., "3D Characterization of the Refractive-Index and Residual-Stress Distributions in Optical Fibers," in *Frontiers in Optics 2012*, paper FTh3C.2.
- [8] Feng, T., Jenkins, M. H., Yan, F., and Gaylord, T. K., "Joint Residual Stress/Refractive Index Characterization of Large-Mode-Area Erbium-Doped Fibers," *IEEE Journal of Lightwave Technology* 31(14), 2426-2433 (2013).
- [9] Feng, T., Jenkins, M. H., Yan, F., and Gaylord, T. K., "Arc fusion splicing effects in large-mode-area single-mode ytterbium-doped fibers," *Applied Optics* 52(32) 7706-7711 (2013).
- [10] Kak, A. C. and Slaney, M., [Principles of Computerized Tomographic Imaging], SIAM 49-112 (2001).
- [11] Yablon, A. D., "Multifocus tomographic algorithm for measuring optically thick specimens," *Optics Letters* 38(21), 4393-4396 (2013).
- [12] Yablon, A. D., "New transverse techniques for characterizing high-power optical fibers," *Optical Engineering* 50(11), 11603 (2011).
- [13] Smith, S. W., [The Scientist's and Engineer's Guide to Digital Signal Processing], California Technical Publishing 442-450 (1997).
- [14] Ramachandran, G. N. and Lakshminarayanan, A. V., "Three-dimensional Reconstruction from Radiographs and Electron Micrographs: Application of Convolutions instead of Fourier Transforms," *Proceedings of the National Academy of Sciences* 68(9), 2236-2240 (1971).
- [15] Yablon, A. D. and Jasapara, J., "Hyperspectral optical fiber refractive index measurement spanning 2.5 octaves", *Proc. SPIE* 8601, (2013).
- [16] Yablon, A.D., "Tomographic Algorithm for Transverse Measurement of Multi-Core and Microstructured Optical Fibers," to be presented at OFC2014, San Francisco, CA, March 12, 2014.